Proceedings of the ASME 2022 41st International Conference on Ocean, Offshore & Arctic Engineering
OMAE 2022
June 5-10, 2022, Hamburg, Germany

OMAE2022-80645

OFFSHORE WIND FARMS AND ISOLATED OIL AND GAS PLATFORMS: PERSPECTIVES AND POSSIBILITIES

Daniel dos Santos Mota[1], **Erick Fernando Alves**[1], **Santiago Sanchez-Acevedo**[2]
Harald G. Svendsen[2], **Elisabetta Tedeschi**[1,3]

[1] Norwegian University of Science and Technology (NTNU), Trondheim, Norway
[2] SINTEF Energi AS, Trondheim, Norway
[3] University of Trento, Trento, Italy

ABSTRACT

Single-cycle gas turbines operating at low-efficiency ranges due to redundancy concerns in offshore oil and gas platforms are responsible for considerable amounts of nitrogen oxides and greenhouse gas emissions in some countries. The abundant resource of offshore wind energy constitutes an extraordinary opportunity for reducing such emissions. However, new challenges are introduced when gas-powered generation is partially replaced by wind power. This paper investigates the possibilities provided by a centralized hybrid energy storage system (ESS) for addressing these challenges. It reviews frequency control concepts for isolated grids and discusses the analogous problem of power balancing within the ESS itself. A set of structures for control of the grid frequency and the ESS DC voltage are described and evaluated. All illustrated by results obtained within the frameworks of the Innovative Hybrid Energy System for Stable Power and Heat Supply in Offshore O&G Installation Project and the LowEmission Research Centre.

1 INTRODUCTION

Rapid climate change is among the biggest global challenges today. The general road-map to tackle this challenge includes country-specific paths that depend on the types of national energy resources. The petroleum sector accounts for a considerable part of nitrogen oxides (NO_x) and greenhouse gas (GHG) emissions of many countries and, at the same time, is a key element of their socio-economic development. In Norway, for instance, 20% of the GHG emissions come from gas turbines (GTs) in operation in the oil and gas (O&G) fields in the Norwegian Continental Shelf [1]. A similar situation with considerable emissions from the offshore O&G sector is observed in other European states, such as the United Kingdom [2] and the Netherlands [3].

Feasible approaches for reducing emissions related to offshore O&G production include the optimization of energy efficiency, carbon capture and storage, electrification from cleaner sources located onshore, and use of renewable energy sources. In this context, the abundant resource provided by offshore wind [4] is extremely promising when economic and environmental aspects are considered. However, technical challenges shall be addressed when integrating wind energy to the isolated power system of an O&G platform. Such platforms rely, typically, on compact single-cycle aeroderivative turbines for electricity generation [5]. Those turbines operate at a relatively stable load, however out of their best efficiency points due to redundancy requirements. Introducing a new but intermittent energy source as wind has positive and negative consequences for the GTs [6, 7]. Among the consequences, one can mention:

- $(+)$ operation of one GT at a higher load and better efficiency range if the redundant one can stay in cold standby;
- $(-)$ increased number of start-stop operations and more variable load profile for the GTs, i.e., higher wear and tear and NO_x emissions;
- $(-)$ overall degradation of the electric power quality and grid frequency stability, resulting in higher wear and tear of motors without variable frequency drives.

To address these issues, one of the solutions investigated by the LowEmission Research Centre (LowEmission) and the Inno-

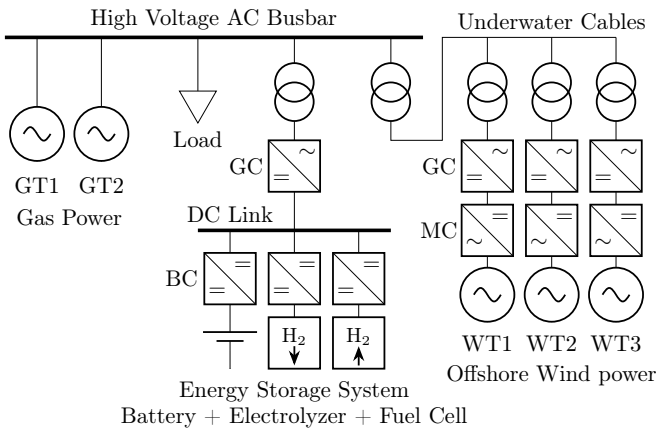

FIGURE 1: PROSPECTIVE SCENARIO OF A WIND FARM AND ESS CONNECTED TO AN EXISTING ISOLATED O&G PLATFORM, ADAPTED FROM [11].

vative Hybrid Energy System for Stable Power and Heat Supply in Offshore O&G Installation Project (HES-OFF) is a centralized hybrid energy storage system (ESS) connected directly to the platform's main alternate current (AC) busbar, as illustrated in Fig. 1. This system combines a slow energy storage device (ESD) composed of an electrolyzer and a fuel cell to counteract wind speed variations on the scale of minutes to hours. Batteries are employed as a fast ESD for the short-term wind speed and load changes. All these ESDs operate in direct current (DC) and are interfaced to the AC grid via a bidirectional AC-DC converter.

The diagram in Fig. 1 stems from a prospective scenario involving an existing O&G platform isolated from the continental electrical grid. This platform is fed by two 35 MW gas-powered generators. Currently, it does not feature an ESS and is not connected to any renewable energy source. A techno-economical assessment [7] estimated that a reduction of approximately 30 % in GHG emissions would be possible if the platform were connected to a 12 MW offshore wind farm (WF). With this assessment as background, a novel sizing methodology for ESSs was proposed in [8]. A set of simulation models [9] of the platform and prospective WF were developed to validate the sizing methodology. These models were further developed [10] and are used in this paper for illustrating fundamental concepts and evaluating the dynamic behavior of the ESS.

In summary, this paper focuses on the frequency control of an isolated O&G platform equipped with a centralized hybrid ESS and connected to an offshore WF. The overall mechanical and electrical power balancing problem of the platform is discussed from a fast frequency support perspective. The analogous electrical power balancing issue of the ESS is also presented. A control strategy applied to the ESS for AC frequency support is described. This strategy is based on established proportional, integral, and derivative (PID) techniques. It does not rely on fast communication links between different ESDs or with the platform's power management system (PMS). Potential challenges are identified and future research paths are discussed. All this is illustrated by previous and current results obtained by HES-OFF and LowEmission research projects.

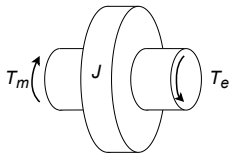

FIGURE 2: AGGREGATED ROTATING MASS MODEL, ADAPTED FROM [12, 13].

2 FREQUENCY CONTROL IN ELECTROMECHANICAL SYSTEMS

The control of the frequency of an AC electrical grid is, essentially, a torque balancing problem. Fig. 2 shows a simplified model of the dynamic behavior of the platform's electromechanical power system [12, 13]. A flywheel with moment of inertia J represents the aggregated rotating masses of the system. The GTs supply mechanical torque T_m to the drive side of the rotating mass. The aggregated electrical loads exert T_e contrary to T_m. The rate in which the angular frequency (ω) changes when a torque imbalance occurs is limited by the system's rotational kinetic energy $E_k = J\omega^2/2$. When expressed in terms of power, the balance of the torques in the system becomes:

$$\underbrace{\omega J \frac{\mathrm{d}\omega}{\mathrm{d}t}}_{\text{Rotating Mass}} = \underbrace{P_m}_{\text{Turbine}} - \underbrace{P_e}_{\text{Loads}} \tag{1}$$

where P_m is the mechanical power delivered by the GTs and P_e is the electrical power consumed in the grid.

A common procedure among power system engineers is to normalize Eqn. (1). This is performed by dividing both sides of the equation by the total apparent power of the generators S_n in VA and by re-writing the moment of inertia J in terms of the inertia constant H [12]:

$$H = \frac{E_{kn}}{S_n} = \frac{J\omega_n^2}{2S_n} \quad [\mathrm{s}] \tag{2}$$

where ω_n is the rated angular frequency of the grid. The constant H is equal to the rated rotating kinetic energy E_{kn} divided by the rated apparent power S_n, which results in a measure of time in seconds. This normalized figure is useful for comparing the relative inertia contribution of different generators.

Replacing gas-powered generation by wind power makes the electrical system of an isolated O&G platform less stable from a frequency control perspective. The reason is that modern wind turbines (WTs) are equipped with full scale back-to-back power

electronic converters (PECs) [14,15,16]. Those do not contribute with mechanical torque T_m to the aggregated rotating mass of the model shown in Fig. 2. Indeed, the power produced by a WT can be modeled as a negative load. In other words, a higher percentage of wind generation means lower electrical torque T_e, not higher T_m. Furthermore, the WTs do not contribute to the aggregated J of the model either [17]. Therefore, every GT that is replaced results in a smaller aggregated kinetic energy buffer E_k. The lower the value of this buffer, the faster the remaining GTs shall respond during disturbances to the power system. However, restrictions in ramping rates and delays of actuators in GT governors limit how fast they can contribute to frequency control. A more in-depth analysis of these limitations and the different strategies and time scales of frequency control are presented in the following section.

2.1 Phases of the Frequency Control

Governors continuously adjust the mechanical power output of GTs to maintain the frequency at its rated value. Fig. 3 illustrates the typical phases of the frequency control after a sudden large power imbalance with excess load. The inertial response phase begins at time $t = 0\,\text{s}$ with the drop in ω at a given rate of change of frequency (RoCoF). The primary phase starts when the governors are able to react to the frequency change. They respond by increasing the power generation which stops the frequency fall. The minimum value reached by ω is known as nadir. During the primary phase, the frequency is raised to a level closer to the rated value. Subsequently, the frequency increases slowly back to the rated value during the secondary response phase. After that, a PMS can decide to slowly replace the power reserves used for frequency control by more efficient measures. This is typically achieved through redispatching of generators and loads in the tertiary response phase. The time scales of the frequency control phases are typically: a few seconds for the inertial, seconds to few minutes for the primary, minutes for the secondary, and from a quarter to a full hour for tertiary [17, 18].

In the next sub-sections, the frequency control phases and their relationship to the inertia and governor responses will be further explained. Though, it is important to emphasize that these descriptions assume that the simplified model in Eqn. (1) is valid. This model assumes that the electrical frequency and the mechanical angular velocity are equivalent. It also assumes that the electrical frequency is a single, global variable that can be used to measure power imbalance. On one hand, the electrical frequency of a country or continent-wide electrical grid is not a single global variable, as shown by real life measurements of the European system [19]. On the other hand, this is still a good approximation for the isolated O&G platform scenario under study and for the time scales investigated in this paper. Therefore, the mechanical angular velocity of the aggregated mass and the electrical angular frequency across the whole platform are assumed to be described by the single global variable ω. The validity of this assumption is assessed later in Section 4. The reader can find a deeper discussion about this issue in [20].

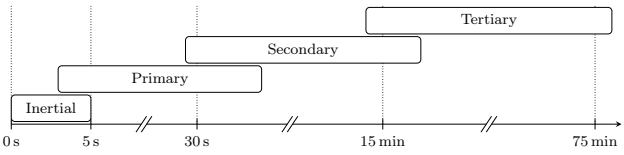

(a) Time scales of the frequency response phases, adapted from [17].

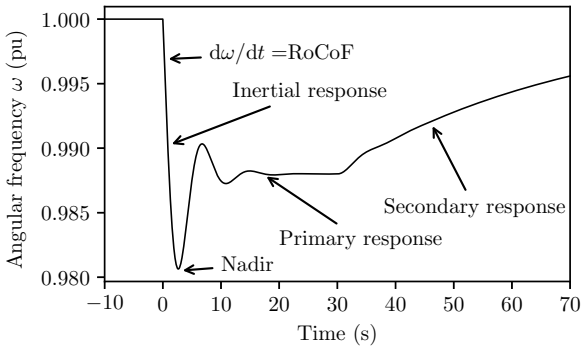

(b) Initial stages after a power imbalance with excess load, adapted from [17, 18], source model and dataset at [10].

FIGURE 3: FREQUENCY RESPONSE PHASES.

2.1.1 Inertial Response

Fig. 4 shows the response of two conceptual systems modeled according to Eqn. (1). The models and dataset are publicly available at [10]. The systems are identical with a single turbine and generator unit connected to an electrical load, except for the levels of inertia which are $H = 5\,\text{s}$ and $H = 10\,\text{s}$. All measurements are in per unit (pu). Figs. 4b, 4d, and 4f represent three components of the electrical power supplied by the generator to the load. The inertial component is provided directly by the rotating mass, no controller needed. The primary and secondary powers are provided by the turbine to the generator.

The power consumed by the load is shown on Fig. 4a. The frequency of the system is initially at equilibrium. On Fig. 4e, the total energy stored in the rotating mass of the high and low inertia cases are shown. At instant $t = 10\,\text{s}$, the electrical load increases in a step from 0.26 pu to 0.38 pu. Immediately after the step, the rotating mass delivers the totality of the power imbalance, i.e., 0.12 pu of power. This is seen on Fig. 4b. Consequently, the level of energy in the buffer (Fig. 4e) begins to drop in conjunction with the frequency (Fig. 4c). Remark that energy is proportional to the square of the frequency.

The inertial response is dominated by the kinetic energy buffer of the rotating masses of the system. This contribution limits the RoCoF. Note that the smaller the buffer, the steeper the RoCoF. Furthermore, the lower the inertia, the lower the nadir.

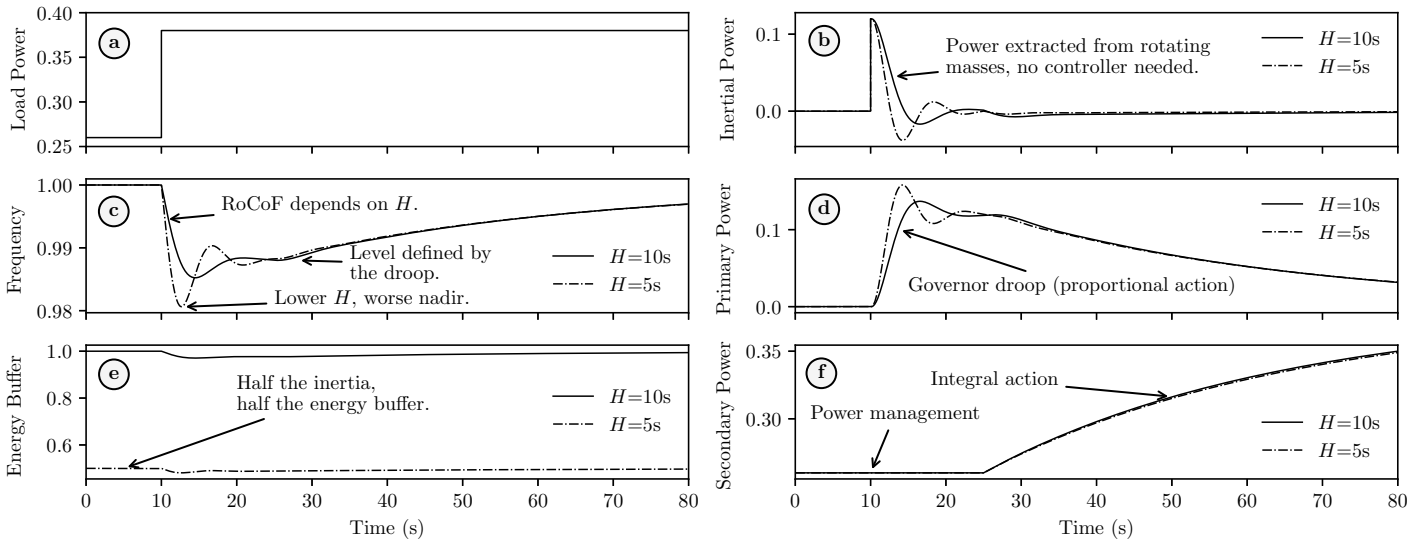

FIGURE 4: INERTIA AND GOVERNOR ROLES IN THE FREQUENCY CONTROL, SOURCE MODEL AND DATASET AT [10].

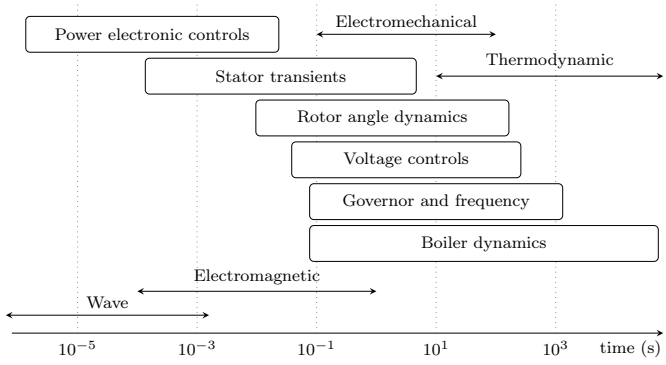

FIGURE 5: CONTROL DYNAMICS IN AC ELECTRICAL SYSTEMS, ADAPTED FROM [18].

2.1.2 Primary Response

The primary response to a power imbalance is shown in Fig. 4d. Once the frequency begins to drop, the turbine governor reacts proportionally to the frequency deviation, i.e., proportionally to $\Delta\omega = \omega_n - \omega$, where ω_n is the rated grid frequency. This action is commonly known as frequency droop [21]. The speed in which the power reacts to the frequency deviation is heavily limited by mechanical constraints of governors and turbines, namely ramping rates and delays of actuators [22]. The higher the actuator delay or the lower the ramping rate, the larger will be the overlap between the inertial and primary responses.

In both high and low inertia cases in Fig. 4, the droop is the same. Therefore, despite featuring different nadirs, the primary response brings the frequency back to the same level for $H = 5\,\mathrm{s}$ and $H = 10\,\mathrm{s}$ (Fig. 4c). As with any other purely proportional regulator with a non-zero set point, a steady-state error between the set point and the controlled variable is always present [23].

2.1.3 Secondary Response

Initially, the turbine and load power were at equilibrium, see Figs. 4a and 4f. This was achieved by the action of the PMS on the secondary power. This response is characterized by an integral action. In an isolated O&G platform, the secondary response is typically performed by a PMS which sends commands to the turbine governors. In large electrical systems, this power management receives the name of automatic generation control [21]. Nevertheless, if there is only one single generator in the system, the secondary control can be performed directly in the governor by an integral regulator [13].

2.2 Other Dynamics

An isolated O&G platform is a power intensive industrial installation with numerous loads as pumps, compressors, and heaters that may or not be interfaced by PECs. A constellation of control loops directly or indirectly connected to each other is necessary to keep the electrical system of a platform in operation. As illustrated by Fig. 5, these controllers operate in different time scales. Traditional voltage regulators and speed governors of synchronous generators work in time scales from 10^{-1} to 10^{3}s. The control structures of modern PECs operate in time scales down to 10^{-5}s or lower [18]. On one hand, these faster responses may be beneficial and add new possibilities for frequency control, such as inertia emulation and other forms of fast regulation [22]. On the other hand, detrimental interactions may also be introduced.

For instance, offshore WTs feature low-frequency oscillation modes due to the slow swinging of their tall floating towers [24]. These low-frequency mechanical oscillations, ulti-

mately, are reflected as variations in the power delivered by the WT to grid. In a large WF with several WTs, these low frequency oscillations can be evened out. However, in the scenario under study in this paper with a few WTs, they might not be negligible. Combined with short-term and long-term wind variations, low frequency power oscillations from the WF increase the burden of GTs for controlling the frequency. Therefore, wear and tear of the GTs and their governors can increase.

3 HYBRID ENERGY STORAGE SYSTEM

Power and energy demands of the frequency control phases are different. Secondary reserves require the largest energy storage, followed by primary reserves and by inertial support. However, inertial support demands the steepest rates of change of power, followed by primary and the secondary reserves. Today's energy storage solutions vary considerably in peak power capacity, rate of change of power limitations, and energy density. There is no one-size-fits-all ESD that is able to store the necessary energy, provide the required peak power, and change the power as fast as required to provide frequency control support during all phases. Therefore, hybrid solutions combining different types of ESDs are becoming a preferred choice in transportation and in power system applications [25].

To address the issues caused by wind intermittency and combine the specific characteristics of different ESDs, LowEmission and HES-OFF investigated the implementation of a centralized hybrid ESS connected directly to the platform's main AC busbar. An example of such system is shown in Fig. 6a. Electrolyzer and fuel cell provide secondary reserves for the frequency control. Batteries are employed as a fast ESD for the short-term variations supplying inertial support and primary reserves. The ESDs operate in DC and are interfaced to the grid via a bidirectional AC-DC converter. A filter stage and a transformer connect the ESS to the platform's main high-voltage (HV) busbar.

Sizing the ESDs and the grid converter (GC) for frequency support in an isolated AC power system is an involved and iterative process. A sizing method [8] has been proposed within the frameworks of LowEmission and HES-OFF. The dataset and models used in this work are available at [9]. Moreover, a hardware-in-the-loop testbed for PECs and ESDs is currently under development for validating the method and for studying the dynamic behavior of a hybrid ESS. Not least, it is worth emphasizing that the proposed method is algebraic and requires the knowledge of a few parameters of the AC power system. Hence, it can be integrated into broader techno-economical optimization algorithms evaluating an installation from a holistic perspective, such as the multi-carrier offshore energy hub approach being developed under LowEmission [26].

3.1 Power Balancing Within the ESS

As previously discussed in Section 2, the frequency control of the platform's AC electric system is a power balancing problem. The power required by the industrial processes and supplied by generators must be continuously equalized. Albeit in a different time scale, the ESS features an analogous power balancing problem.

At the core of the ESS shown in Fig. 6a, in the DC link, there is a capacitor bank represented by C_{dc}. Similarly to the rotating masses of the AC grid, the capacitor bank holds an energy buffer $E_e = {}^{C_{dc}\, v_{dc}^2}/_2$. Moreover, variations in the dc-link voltage (v_{dc}) indicate a power imbalance between the ESDs and the AC-DC converter. In other words, if the power supplied by the ESDs and the power transferred from the DC link to the AC grid by the GC are in equilibrium, the voltage at C_{dc} is constant. If the net power supplied to the DC link is positive, v_{dc} increases in conjunction with the energy E_e. Conversely, if the net power is negative, v_{dc} decreases. Assuming that losses on the converters and DC link of the ESS are negligible, the dynamic behavior of v_{dc} described in terms of the currents i_{es} and i_{gcd} is

$$\underbrace{C_{dc}\frac{\mathrm{d}v_{dc}}{\mathrm{d}t}}_{\text{Buffer}} = \underbrace{i_{es}}_{\text{From ESDs}} - \underbrace{i_{gcd}}_{\text{To AC side}} . \tag{3}$$

Alike a turbine governor controlling the AC grid frequency, the ESS shall contain an internal DC voltage controller acting either on the ESD or GC power flow to constrain v_{dc} variations. Naturally, this DC voltage control happens in a fraction of the time scales for frequency control described in Section 2. Failure to do so may result in voltage collapse of the ESS or significant power oscillations. Though, note that the larger the capacitance C_{dc}, the larger the energy buffer E_e and the more forgiving the system is to unbalances between the ESDs and GC. Therefore, sizing C_{dc} becomes a techno-economical task that has consequences to the tuning and dynamics of the DC voltage controller. This issue is among the topics discussed in the algebraic method for sizing the ESS proposed in [8].

In this backdrop, a set of structures for the AC frequency support and the internal v_{dc} control have been adopted within the scope of LowEmission and HES-OFF projects. In the next section, these structures are presented.

3.2 ESS Control Structure

In this section, the main control structures employed in the battery converter (BC) and GC are presented. The term battery is used for ESDs in general. So, the concepts are also applicable to fuel cells and electrolyzers with only minor adaptations. It is also important to emphasize that an approach based on traditional PID controllers is adopted for the hybrid ESS proposed in this paper. This choice was made because those are well-proven and usually available in commercial products. Moreover, a structure that does not rely on a fast communication link between the different converters of the ESS or with the platform's PMS is chosen. Finally, all PECs of the ESS operate with a pulse-width

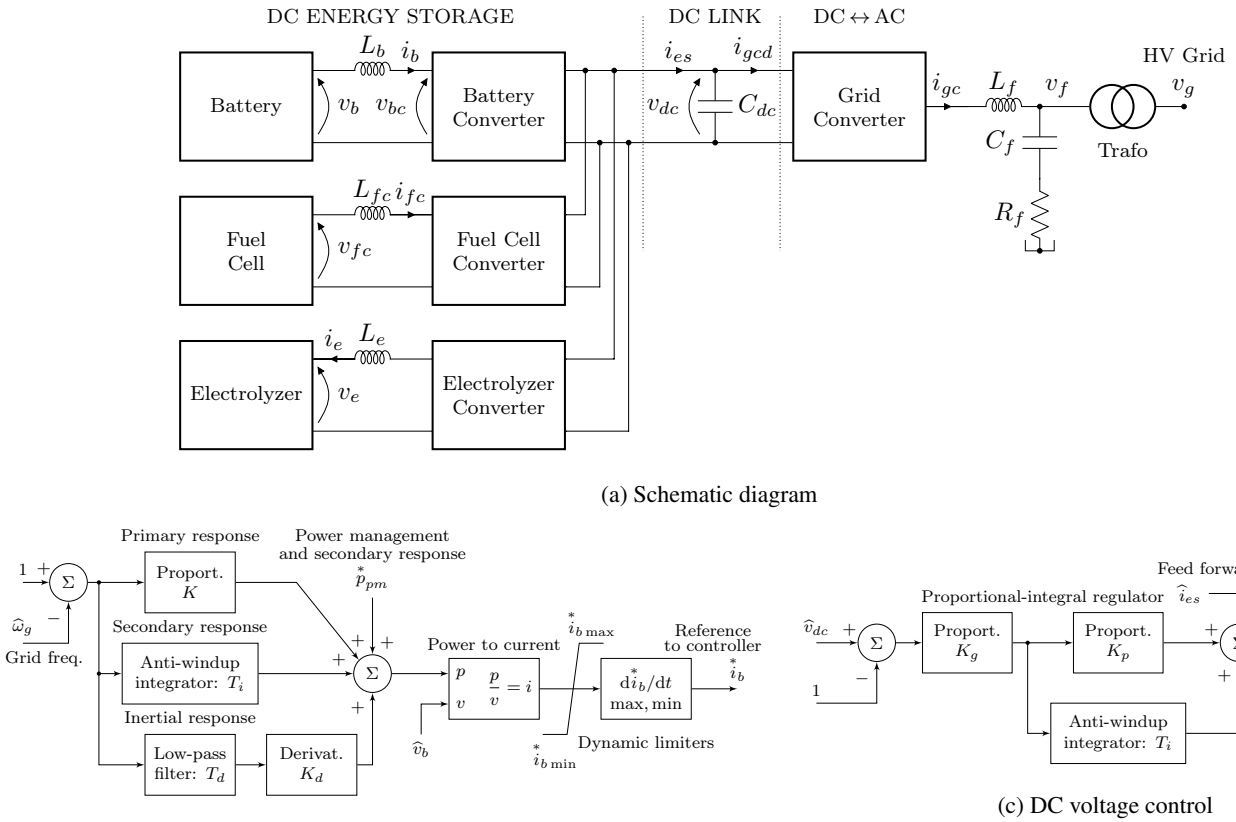

(a) Schematic diagram

(b) Grid frequency control

(c) DC voltage control

FIGURE 6: HYBRID ENERGY STORAGE SYSTEM.

modulation (PWM) technique, see [27] for more information on this topic. They use cascaded control structures with a fast inner current control loop and a slower outer loop. The outer loops control variables are the grid angular frequency (ω) and the DC-link voltage (v_{dc}) as seen in Fig.6.

3.2.1 Grid Frequency Control

Fig. 6b shows the control structure for the AC frequency support provided by the ESS. The dynamic behaviour of this structure will be assessed later in Section 4.1. Moreover, the structure uses the measurement of the grid frequency $\widehat{\omega}_g$ to generate the reference $\overset{*}{i}_b$ for the BC inner current control loop. Remark that all measurements (denoted as $\widehat{x}$) in the control structures are assumed to have been properly conditioned, filtered, and scaled. The structure is divided into three branches that correspond to the different phases of the frequency control of AC grids.

- **Primary response**: proportional gain K. It is the equivalent of the inverse of the droop. The higher the gain K, the higher the contribution of the battery for a given grid frequency deviation.
- **Secondary response**: integrator time T_i and input for power reference $\overset{*}{p}_{pm}$. If the BC is the only device in the system supplying secondary reserves, the integral branch can be enabled. This branch works towards removing the steady-state error left by the droop based control. However, if a GT or another ESD is also a source of secondary reserves, the T_i branch is disabled. Then, the input $\overset{*}{p}_{pm}$ is used by the PMS to coordinate the delivery of reserves between GTs and ESDs. Moreover, $\overset{*}{p}_{pm}$ is also the input for controlling the state of charge (SOC) of the battery.
- **Inertial response**: derivative gain K_d. Contrary to the "real" inertial response provided by rotating masses, the inertia emulation from the battery relies on a frequency measurement which is inherently noisy. Therefore, a low-pass filter stage with a time constant T_d is necessary in the derivative branch.

The minimum and maximum values ($\overset{*}{i}_{b\max}$ and $\overset{*}{i}_{b\min}$) in Fig. 6b provide the means for dynamically limiting the operation based on SOC, temperature, or other conditions of the ESD. The rate-of-change limiters are not necessarily static nor symmetric. Moreover, the "power to current" block compensates for variations in the battery voltage. This compensation, however, is not yet implemented in the results shown later in Section 4 as it can be detrimental to the battery health during large charge or

discharge power variations. Besides, it adds a non-linearity in the control loop that is known to cause instabilities when the BC is heavy loaded [28]. Another method to reach this compensation is implementing a proportional and integral (PI) controller for active power control. This alternative adds another layer of control, and consequently reduces the frequency control bandwidth, which might also cause stability problems. Hence, this is a topic currently under investigation in LowEmission.

3.2.2 DC Voltage Control

The GC adopted for the ESS is composed of a two-level three-phase insulated-gate bipolar transistor bridge. A passive inductive-capacitive-inductive (LCL) filter connects the GC to the grid, see Fig. 6a. This filter employs a reactor (L_f) and a capacitive-resistive branch (C_f and R_f). The second inductive device is the transformer. See [29] for more information on passive LCL-filters.

The GC operates as a three-phase voltage source. With the help of PWM switching and the LCL-filter, the converter is able to synthesize three-phase sinusoidal currents (i_{gc}). The traditional inner current control in a rotating reference frame (RRF) is adopted. This strategy relies on the measurement of the phase of the AC voltage with a phase-locked loop (PLL). See [30] for a literature review on PLLs. A set of mathematical operators is used to transform the measured three-phase voltages and currents to a direct and quadrature reference frame [31]. When the angular frequency of the RRF matches the angular frequency of balanced three-phase voltages and currents, the direct and quadrature values become constant. This allows the use of two sets of PI regulators for controlling the AC current of the converter [32]. Moreover, the GC direct-axis current (i^d_{gc}) produces active power. Whereas, the quadrature-axis current (i^q_{gc}) produces reactive power.

Fig. 6c shows the DC voltage control loop of the GC. It has the measurement of the DC-link voltage $\widehat{v}_{dc}$ as an input. The direct current reference $\overset{*}{i}{}^d_{gc}$ is sent to the converter's fast inner current controller. For improving the DC-voltage dynamics, a feed-forward path ($\widehat{i}_{es}$) is provided for the total current from the ESDs. This, however, does not represent a need for fast communication between the BCs and the GC. If a DC-current measurement transducer is connected at the electrical point marked by i_{es} in Fig. 6a and interfaced with the GC controller, then no direct communication with the different ESDs is necessary.

It is worth mentioning that the performance of current controllers in RRF is affected by unbalanced three-phase loads, i.e., when the loads on each of the phases of the system are considerably different. Within the scope of LowEmission and HES-OFF, a strategy known as dual-sequence current controller has been investigated. This strategy relies on splitting three-phase measurements into two components, one called positive and the other negative sequence. These components are different RRFs with opposite angular speeds. A literature review and a comparison of controllers with two different sequence separation strategies was done in [11]. An improved method for sequence separation was proposed in [33]. Nevertheless, the operation under unbalanced conditions is considered outside the scope of this paper.

4 PERSPECTIVES AND POSSIBILITIES WITH A HYBRID ESS

In this section, an analysis of the possibilities provided by a hybrid ESS is presented. Some of the challenges from the perspective of a power system engineer are also discussed. The results of computer simulations are used as illustration. The simulation models used herein have been developed under the frameworks of LowEmission and HES-OFF. The base models [9] were programmed originally in MATLAB R2016a. However, for this paper, these were re-written in DIgSILENT PowerFactory 2020 SP2A. The re-written models are available at [10].

The single line diagram in Fig.1 represents the test cases. Two gas-powered generators are connected to the platform's main HV busbar. A set of general loads represent the total electrical consumption on the platform. Three type 4 [14] offshore floating WTs are connected to the main busbar via an HV underwater collector system. PowerFactory's detailed model with PWM switching with built-in fast current controllers in the RRF [34] are used for the GCs of the ESS and WTs. A simplified average model of the ESD converters is used. For details on PECs modeling strategies, see [35]. The converters' outer loops from Figs. 6b and 6c were manually programmed in PowerFactory. Three cases are used for analysis and discussion in this section:

- case 1: ESS is connected but does not provide support for frequency control;
- case 2: ESS provides primary support;
- case 3: ESS provides inertial and primary support.

In all cases, two GTs and the WF are feeding a base load of 46 MW. Each WT produces 4 MW. At instant $t = 1$ s, a step load of 4 MW is applied to the platform's HV busbar. Both turbine governors run in speed control with a droop of 4.7 %. The rated power of the ESS GC is 10 MVA and the rated power of the ESS' BC is 4 MW. The ESS fuel cell converter (FCC) rated power is 6 MW. The FCC is set to supply a slow secondary response to frequency variations. This secondary response is, however, not significant within the time scales of the three cases.

4.1 Frequency Support Provided by the ESS

Fig. 7 shows the response to the step load transient. On Fig. 7a, the total electrical load of the platform is shown. The transient causes a sudden dip in the platform's busbar voltage (Fig. 7f). There is room for improvement if an AC voltage support control structure were implemented in the ESS as discussed in [36]. The power supplied by the generators is shown on Fig. 7e. For case 1 (no ESS support), the two generators supply

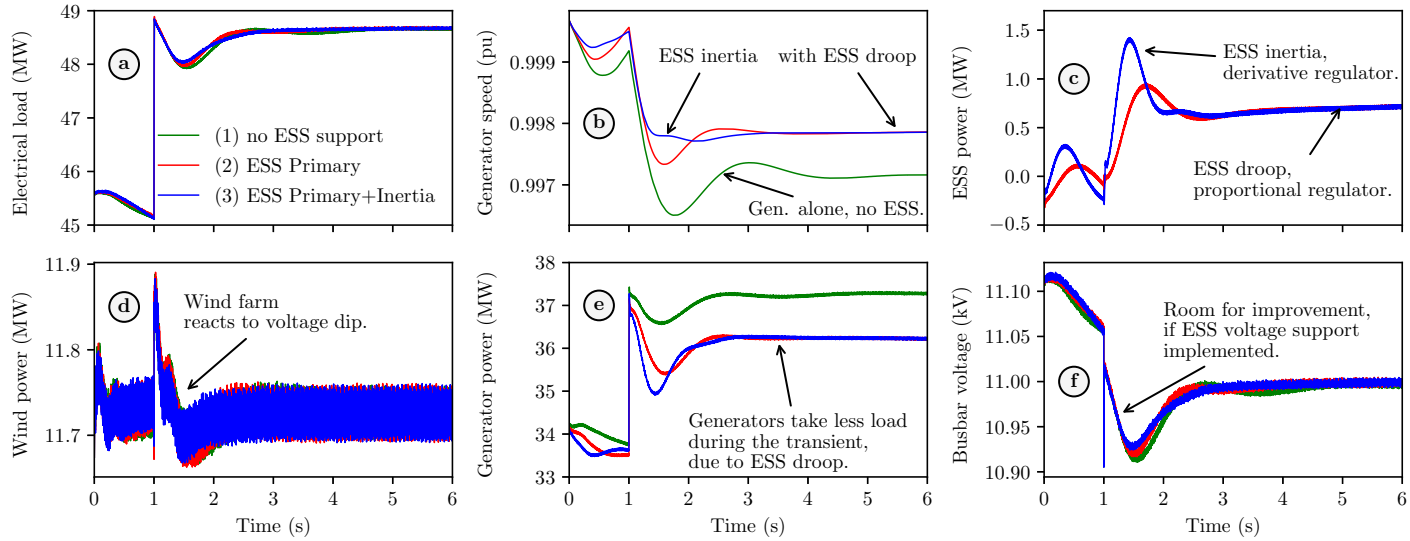

FIGURE 7: ESS PROVIDING INERTIA AND PRIMARY RESERVES, SOURCE MODEL AND DATASET AT [10].

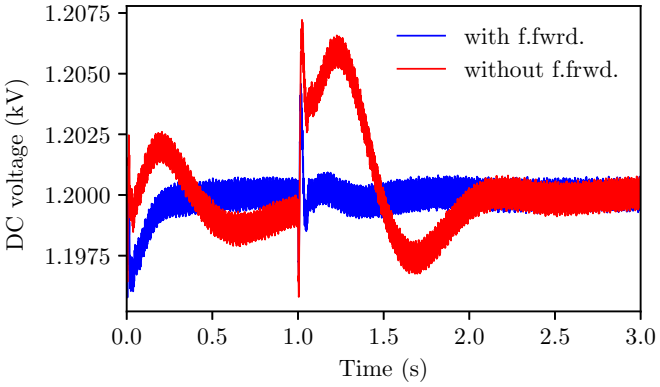

FIGURE 8: CASE 3, DC VOLTAGE WITH (BLUE) AND WITHOUT (RED) FEED-FORWARD SCHEME.

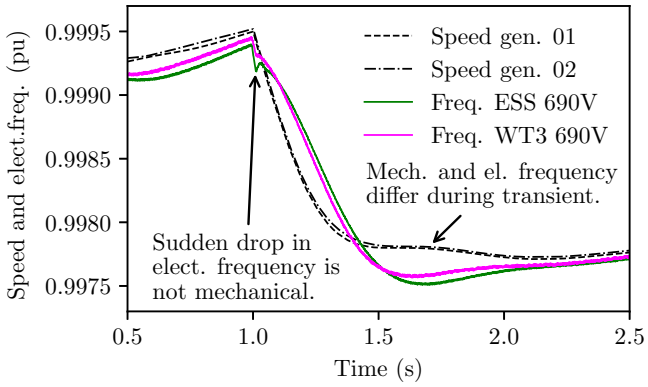

FIGURE 9: CASE 3, MECHANICAL SPEED AND ELECTRICAL FREQUENCY.

all the extra power demanded by the step load. When droop and inertial support is provided by the ESS, the BC assumes part of the load. The next research step within the LowEmission project is to investigate scenarios where most of the primary frequency reserve is provided by the ESS, not by the GTs.

4.2 DC Voltage Control within the ESS

Fig. 8 shows the effect on the DC voltage of operating with or without the feed-forward scheme during the transient with ESS inertial and primary support (case 3). It is clear that the DC voltage control becomes worse without the feed-forward scheme. The differences are, however, considerably small. Nevertheless, the lower the capacitance connected to the DC link, the higher the DC voltage variations will be during transients. Therefore, the improved dynamic provided by the feed-forward can be more suited when a reduction of the capacitance bank is desirable. Reducing the capacitance bank and improving the DC voltage regulators are future research paths that might be taken within the scope of LowEmission and HES-OFF.

4.3 Frequency as a Global Variable

In Section 2, the electrical frequency across the whole platform and the mechanical speed of the GTs are treated as one unique variable. A comparison is made for case 3 to test the validity of the "global variable" assumption. Fig. 9 shows, in pu, the speed of the GTs and the electrical frequency at the low-voltage (LV)-side of the ESS transformer (ESS 690V) and at the LV-side of the WT3 transformer (WT3 690V). The WT number 3 is the one furthest from the platform. The electrical measurement is performed with PowerFactory's built-in PLLs [34]. The mechanical speeds of the GTs are almost identical. There is, on the other hand, a noticeable difference between the mea-

sured electrical frequencies and the mechanical speeds. Moreover, the sudden change in the voltage profile at the platform's HV busbar (not shown in the curves) caused by the step load is detected by the PLL at the LV-side of the ESS transformer as a small but sharp frequency dip. For WT3, which is farther from the transient source, the measured electrical frequency features a smoother dip. An ESD with supercapacitors providing inertial support might respond to such dip. Investigating this issue is one of future research paths within the scope of LowEmission.

5 FUTURE RESEARCH

A centralized hybrid ESS can be used to alleviate the negative consequences of connecting an intermittent energy source to an isolated electrical system. However, this concept still poses challenges which deserve further investigation. Some of these challenges were identified and discussed in this paper. Among them, the following open topics can be highlighted.

- **DC voltage**: the feed-forward scheme described in this paper may play an important role in a future optimization of the DC-link capacitor bank sizing and, consequently, in the GC cost, weight, and space requirements.
- **AC voltage**: the ESS is capable of providing reactive power support reducing voltage sags and swells during transients. Nevertheless, fast interactions between the ESS converters, other large PECs in the platform, and WTs shall be further assessed.
- **Primary reserves**: in the scenario analysed in this paper, both the GTs and the ESS were providing primary reserves. The limitations and techno-economical consequences of increasingly transferring the primary frequency control from the GTs to the ESS shall be further investigated.
- **Inertial reserves**: electrical transients can produce fast changes in the AC frequency that are not representative of mechanical changes in the rotational speed of the GTs. These fast changes in the electrical frequency can be detrimental to the performance of ESDs providing inertial reserves. Alternative electrical frequency measurement methods and their effects in the dynamics of derivative-based inertial reserves shall be assessed in the future.

6 CONCLUSION

This paper analyzed the possibilities provided by a centralized hybrid ESS for alleviating the negative consequences of integrating an offshore WF to the AC grid of an isolated O&G platform. It presented a set of structures for providing inertial, primary, and secondary reserves to frequency control and for controlling the internal DC voltage of the ESS. These structures are based on established PID techniques and do not rely on fast communication links between the different converters of the ESS nor with the platform's PMS. The proposed concept shows promising results when assessed through publicly available models developed under the frameworks of HES-OFF and LowEmission. Notwithstanding, challenges from a power systems perspective remain open. Some of these challenges were highlighted in this paper and must be further investigated.

ACKNOWLEDGMENT

This research was funded by the Research Council of Norway through the PETROSENTER scheme, under the "Research Centre for Low-Emission Technology for Petroleum Activities on the Norwegian Continental Shelf" (LowEmission), grant number 296207, and through the program PETROMAKS2, grant number 281986, project "Innovative Hybrid Energy System for Stable Power and Heat Supply in Offshore Oil & Gas Installation (HES-OFF)".

REFERENCES

[1] OED, 2022, "Norwegian Petroleum Emissions to Air 2020," Norwegian Ministry of Petroleum and Energy (OED), Oslo, Norway, accessed Feb. 17, 2022, https://www.norskpetroleum.no/en/environment-and-technology/emissions-to-air/

[2] OGUK, 2021, "North Sea Transition Deal," Department for Business, Energy & Industrial Strategy, London, United Kingdom, Report NSTD.

[3] Tamez, A. S. and Dellaert, S., 2020, "Decarbonisation Options for the Dutch Offshore Natural Gas Industry," PBL Netherlands Environmental Assessment Agency and TNO Energy Transition, Report PBL 416.

[4] IEA, 2019, "Offshore Wind Outlook 2019," International Energy Agency, Paris, France, Report WEO STO 2019.

[5] Devold, H., 2013, *Oil and Gas Production Handbook, an Introduction to Oil and Gas Production, Transport, Refining and Petrochemical Industry*, 3rd ed., ABB Oil and Gas, Oslo, Norway.

[6] Korpås, M., Warland, L., He, W., and Tande, J. O. G., 2012, "A Case-Study on Offshore Wind Power Supply to Oil and Gas Rigs," Energy Procedia, **24**, pp. 18–26.

[7] Riboldi, L., Alves, E. F., Pilarczyk, M., Tedeschi, E., and Nord, L. O., 2020, "Optimal Design of a Hybrid Energy System for the Supply of Clean and Stable Energy to Offshore Installations," Frontiers in Energy Research, **8**, p. 346.

[8] Alves, E. F., Mota, D. d. S., and Tedeschi, E., 2021, "Sizing of Hybrid Energy Storage Systems for Inertial and Primary Frequency Control," Frontiers in Energy Research, **9**, p. 206.

[9] Alves, E. F., 2021, "Hybrid ESS Design Repository - Data Set and Simulation Files," DOI: 10.5281/zenodo.4384697.

[10] Mota, D. d. S., 2021, "Data Repository of the Manuscript Offshore Wind Farms and Isolated Oil and Gas Platforms," DOI: 10.5281/zenodo.6095756.

[11] Mota, D. d. S. and Tedeschi, E., 2021, "Understanding the Effects of Exponentially Decaying DC Currents on the Dual dq Control of Power Converters in Systems with High X/R," IEEE, Florence, Italy, 15th International Conference on Compatibility, Power Electronics and Power Engineering, pp. 1–6, DOI: 10.1109/CPE-POWERENG50821.2021.9501204.

[12] Kundur, P., Balu, N. J., and Lauby, M. G., 1994, *Power System Stability and Control*, EPRI Power System Engineering Series, McGraw-Hill, New York, USA.

[13] Machowski, J., 2008, *Power System Dynamics: Stability and Control*, 2nd ed., Wiley, Chichester, U.K.

[14] IEC, 2015, "Wind turbines - Part 27-1: Electrical simulation models," International Electrotechnical Commission, Geneva, Switzerland, IEC Standard 61400-27-1:2015.

[15] Siemens, 2017, "The Top-Performing Wind Converter Trusted Technology for Maximum Power Yield – SINAMICS W180," Siemens AG, Munich, Germany, Brochure PDLD-B10099-00-7600.

[16] ABB, 2020, "ACS880-77LC/-87LC/-87CC Wind Turbine Converters," ABB, Zurich, Switzerland, System Description 3AXD50000022022 Rev C.

[17] Milano, F., Dörfler, F., Hug, G., Hill, D. J., and Verbič, G., 2018, "Foundations and Challenges of Low-Inertia Systems (Invited Paper)," IEEE, Dublin, Ireland, Power Systems Computation Conference, pp. 1–25, DOI: 10.23919/PSCC.2018.8450880.

[18] Hatziargyriou, N., Milanovic, J., Rahmann, C., Ajjarapu, V., Canizares, C., Erlich, I., Hill, D., Hiskens, I., Kamwa, I., Pal, B., Pourbeik, P., Sanchez-Gasca, J., Stankovic, A., Van Cutsem, T., Vittal, V., and Vournas, C., "Definition and Classification of Power System Stability – Revisited & Extended," IEEE Transactions on Power Systems, **36**(4), pp. 3271–3281.

[19] Swissgrid, 2022, "Current Grid Key Figures - Frequency," accessed Feb. 17, 2022, https://www.swissgrid.ch/en/home/operation/grid-data/current-data.html

[20] Caliskan, S. Y. and Tabuada, P., 2015, "Uses and Abuses of the Swing Equation Model," IEEE, Osaka, Japan, 54th IEEE Conference on Decision and Control, pp. 6662–6667, DOI: 10.1109/CDC.2015.7403268.

[21] IEEE Task Force on Turbine-Governor Modeling, 2013, "Dynamic Models for Turbine-Governors in Power System Studies," IEEE Power & Energy Society, Report PES-TR1.

[22] ENTSO-E, 2019, "Fast Frequency Reserve – Solution to the Nordic Inertia Challenge," ENTSO-E / Danske Energinet, Denmark, Report FFR.

[23] Ogata, K., 2010, *Modern Control Engineering*, 5th ed., Prentice-Hall, Boston, USA.

[24] Larsen, T. J. and Hanson, T. D., 2007, "A Method to Avoid Negative Damped Low Frequent Tower Vibrations for a Floating, Pitch Controlled Wind Turbine," Journal of Physics: Conference Series, **75**, p. 012073.

[25] Hemmati, R. and Saboori, H., 2016, "Emergence of Hybrid Energy Storage Systems in Renewable Energy and Transport Applications – A Review," Renewable and Sustainable Energy Reviews, **65**, pp. 11–23.

[26] Zhang, H., Tomasgard, A., Knudsen, B. R., Svendsen, H. G., Bakker, S. J., and Grossmann, I. E., 2021, "Modelling and Analysis of Offshore Energy Hubs," Cornell University arXiv:2110.05868 [cs, eess, math].

[27] Mohan, N., Undeland, T. M., and Robbins, W. P., 1995, *Power Electronics: Converters, Applications, and Design*, 2nd ed., Wiley, New York, USA.

[28] Ibanez, F. M., Martin, F., Eletu, J., and Echeverria, J. M., 2021, "Input Voltage Feedforward Control Technique for DC/DC Converters to Avoid Instability in DC Grids," IEEE Journal of Emerging and Selected Topics in Power Electronics, **9**(5), pp. 6099–6112.

[29] Brantsæter, H., Kocewiak, L., Tedeschi, E., and Årdal, A. R., 2015, "Passive Filter Design and Offshore Wind Turbine Modelling for System Level Harmonic Studies," Energy Procedia, **80**, pp. 401–410.

[30] Golestan, S., Guerrero, J. M., and Vasquez, J. C., 2017, "Three-Phase PLLs: A Review of Recent Advances," IEEE Transactions on Power Electronics, **32**(3), pp. 1894–1907.

[31] O'Rourke, C. J., Qasim, M. M., Overlin, M. R., and Kirtley, J. L., 2019, "A Geometric Interpretation of Reference Frames and Transformations: Dq0, Clarke, and Park," IEEE Transactions on Energy Conversion, **34**(4), pp. 2070–2083.

[32] Blaabjerg, F., Teodorescu, R., Liserre, M., and Timbus, A., 2006, "Overview of Control and Grid Synchronization for Distributed Power Generation Systems," IEEE Transactions on Industrial Electronics, **53**(5), pp. 1398–1409.

[33] Mota, D. d. S., Alves, E. F., and Tedeschi, E., 2021, "Dual Sequence Controller with Delayed Signal Cancellation in the Rotating Reference Frame," Cartagena, Colombia, IEEE 22nd Workshop on Control and Modelling of Power Electronics, pp. 1–8, DOI: 10.1109/COMPEL52922.2021.9646023.

[34] DIgSILENT, 2021, "PowerFactory 2020, Technical Reference," DIgSILENT GmbH, Overview PF2020.

[35] Bacha, S., Munteanu, I., and Bratcu, A. I., 2013, *Power Electronic Converters Modelling and Control with Case Studies*, Advanced Textbooks in Control and Signal Processing, Springer, London, England.

[36] Alves, E., Sanchez, S., Brandao, D., and Tedeschi, E., 2019, "Smart Load Management with Energy Storage for Power Quality Enhancement in Wind-Powered Oil and Gas Applications," Energies, **12**(15), p. 2985.